

Edge-state mediated front propagation in compliant channels

Callum Cuttle, Draga Pihler-Puzović, and Anne Juel*

Manchester Centre for Nonlinear Dynamics and School of Physics and Astronomy,
University of Manchester, Oxford Road, Manchester M13 9PL, United Kingdom

(Dated: December 15, 2024)

Front-propagating systems provide some of the most fundamental physical examples of interfacial instability and pattern formation. However, their nonlinear dynamics are rarely addressed. Here, we present an experimental study of air displacing a viscous fluid within a collapsed, compliant channel a model system for pulmonary airway reopening. We show that compliance induces fingering instabilities absent in the rigid channel and, moreover, that the dynamics of the air-fluid front are dominated by a host of unstable modes over a significant range of experimental parameters.

Morphological growth ranging from tumour angiogenesis [1] and growth [2], to bacterial colonies [3] and electrodeposition [4] is susceptible to interfacial instabilities which can lead to pattern formation and the emergence of disordered dynamics [5]. A canonical example is the viscous fingering instability which occurs when air displaces a viscous fluid in the narrow gap between two rigid parallel plates [6, 7]. Its complex behaviour stems from the nonlinearity of the interface shape, but has yet to be addressed in terms of nonlinear dynamics. In radial geometries, the growth of the interface is disordered with continually-evolving branched structures arising from initially axisymmetric fronts [7]. In contrast, when the flow is confined to a rectangular channel, the system supports a single stable mode of displacement, with planar fronts evolving to a steadily propagating finger of air [6]. Recent work has shown that in a radial cell the instability may be suppressed if one of the plates is replaced by a compliant membrane [8, 9]. In this letter, we show experimentally that in a rectangular channel with an elastic boundary, compliance gives rise to new modes of stable finger propagation characterised by the continual emergence of small scale features at the front of the finger. We find a region of bistability where the transient evolution of the system towards either stable state is mediated by unstable modes of finger propagation. These dynamics are reminiscent of the edge states which separate the laminar from the turbulent state in the subcritical transition to turbulence in shear flows [10] or control droplet break-up in sub-critical extensional flows [11]. We find that the evolution of the interface in our system is directly influenced by edge states over a significant range of experimental parameters.

Related systems have been studied extensively in the context of pulmonary airway reopening [13–17]. Here, bronchioles, initially collapsed and filled with viscous fluid, were modelled as compliant channels or tubes, reopened by the propagation of an injected finger of air which redistributes the fluid. Numerical studies conducted at fixed levels of initial collapse and compliance have consistently reported a generic two-branch push/peel solution in terms of bubble pressure and capillary number Ca , the non-dimensional finger speed [18–

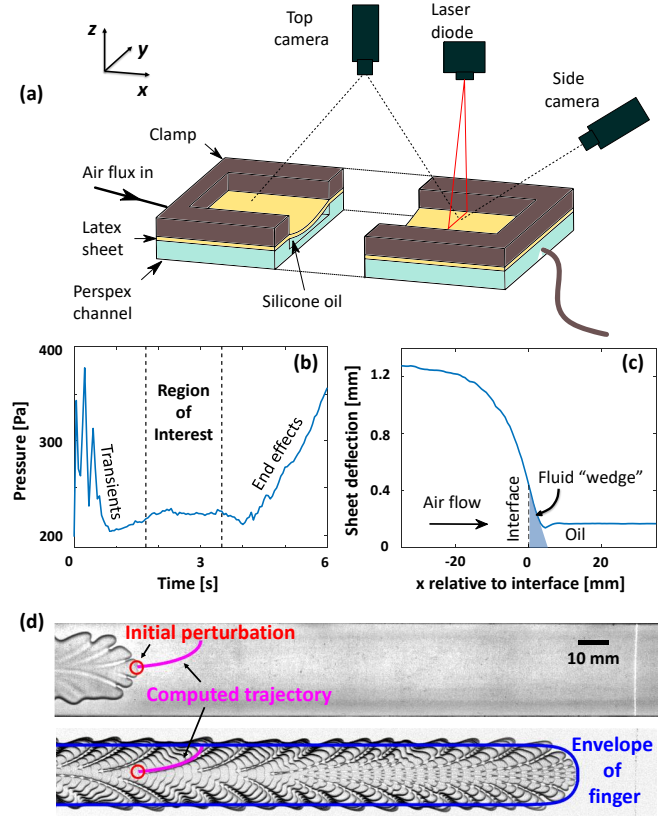


FIG. 1. (a) Schematic diagram of the elasto-rigid channel. (b) Pressure trace for stable finger propagation, with variations of < 10 Pa in the region of interest. (c) Instantaneous reopening profile centered on the position of the air-oil interface. (d) Top to bottom: top-view image of an air finger with short perturbations along the interface; composite image of the same experiment, demonstrating spatio-temporal pattern formation. The envelope of the finger was approximated by [6]. The path of the circled perturbation was fitted following [12], taking the width of the envelope and the initial coordinates of the perturbation as fitting parameters.

20]. For peeling modes, an increase in bubble pressure drives an increase in Ca , while for the pushing modes predicted at low Ca the converse is true – faster reopening occurs at lower pressures. The pushing branch has been

found to be linearly unstable [21] in a two-dimensional (2D) geometry consisting of a planar, flexible-walled channel. Fixing the volumetric flow rate Q and allowing bubble pressure and Ca to vary, gives rise to transient relaxation oscillations on the pushing branch, corresponding to abrupt transitions between pushing and peeling [22].

Three-dimensional steady simulations have imposed symmetry about the two longitudinal midplanes of the tube [20], and so have lacked the multiple propagation modes arising from the fluid-structure interaction flow observed in experiments [14]. In strongly collapsed vessels, novel asymmetric and symmetric modes were associated with two disconnected peeling branches at low and high Ca [14, 15]. Pushing modes, however, have been conspicuously absent in experiments. Here, we report the first experimental observation of a pushing branch, which acts as an edge state between two peeling modes with different symmetries.

The experiments were performed in a Hele-Shaw channel with an elastic upper boundary, as shown schematically in Fig. 1(a). A channel of length 60 cm, width 30.00 ± 0.02 mm and depth 1.05 ± 0.01 mm was milled into a block of Perspex, achieving a roughness of less than $10 \mu\text{m}$ along the base. The upper boundary comprised a latex sheet (Supatex) of thickness 0.46 ± 0.01 mm, Young's modulus $E = 1.44 \pm 0.05$ MPa and Poisson's ratio $\nu = 0.5$. A pre-stress was imposed uniformly along the sheet by hanging evenly distributed weights (3.03 ± 0.01 kg) from one long edge before clamping the sheet over the channel.

Prior to each experiment, the channel was inflated with silicone oil (Basildon Chemicals Ltd.) of viscosity $\mu = 0.099$ Pa s, interfacial tension $\sigma = 21$ mN/m and density $\rho = 973$ kg/m³ at laboratory temperature $21 \pm 1^\circ\text{C}$. The inlet was closed and the oil was allowed to drain via a tube left open to the atmosphere. The initial level of collapse was controlled via the hydrostatic pressure difference between the channel and the outlet. In our experiments the channel was strongly collapsed, with the ratio of the transverse cross-sectional area under the elastic sheet to that of the underformed channel fixed at $A_i = 0.44 \pm 0.02$, close to opposite wall contact which occurs at $A_i = 0.36$ [15]. We injected air into the channel at constant volumetric flow rate $10 < Q < 180$ ml/min, which led to the propagation of an air finger inflating the channel. Flow was controlled via a syringe pump (KDS 200) fitted with Gastight syringes (Hamilton), with initial conditions set by a small precursor bubble of air (less than 1 ml) injected immediately before each experiment. The bubble pressure in the air finger was measured with a pressure sensor (Honeywell ± 5 " H₂O), with a typical trace shown in Fig. 1(b). The experimental region of interest (ROI) covered a 250 mm long region over which pressure variations of less than 10 Pa were recorded during steady finger propagation. This level of

accuracy relied sensitively on the uniformity of the pre-stress imposed on the membrane. The air finger was imaged from above by a camera with a spatial resolution of 4.8 ± 0.1 pix/mm, recording 4–30 frames per second (fps), depending on Q . The channel was lit from below. We recorded the position of the tip of the air finger in each frame using image analysis routines (MATLAB 2016a), and calculated the tip propagation speed U between frames. Over the ROI, U typically varied by 5% for steady reopening [top image in Fig. 2(a)]. The deflection of the membrane was measured using a laser sheet projected across the width of the channel at the end of the ROI. This line was imaged at an oblique angle by a second camera (22.9 ± 0.2 pixels/mm; 40-160 fps). Membrane deflection at the midpoint of the channel, along with knowledge of the tip propagation speed were then used to reconstruct the profile of the sheet during reopening, as in Fig. 1(c). Behind the air-oil interface the channel inflates while far ahead the channel is still collapsed; hence, the interface advances into a tapered geometry, behind a wedge-shaped volume of fluid.

The size of this wedge decreases as Ca increases. At high Ca , the interface therefore lies within the strongly tapered region, with a printers'-like instability generating multiple viscous fingering perturbations along the tip [see *e.g.* 23, 24], as in Fig. 1(d). Due to the curvature of the interface, these perturbations are advected away from the tip along trajectories instantaneously normal to the interface as it propagates, consistent with the kinematic boundary condition [12]. Repeated shedding of perturbations produces complex spatio-temporal patterns, which we visualise using composite images generated from successive frames of a top-view recording, as shown in Fig. 1(d). Here, the pink trajectory obtained following [12] provides a close approximation to the path of the circled perturbation. The separation between advected perturbation trajectories reflects the rate at which perturbations were produced at the tip. Observations of pattern formation provided a sensitive measure of bubble pressure and capillary number, defined here as $Ca = \mu U / \sigma$. Small experimental variations in these parameters were clearly reflected in the pattern, and distinct patterns were associated with each mode of propagation.

In our experiments we observed two peeling modes of finger propagation illustrated in Fig. 2 – asymmetric or symmetric about the longitudinal axis of the channel. The taper-induced instability described above is unique to the symmetric peeling modes at high Ca [Fig. 2(b)]. The small-amplitude fingering perturbation which generates this feathered pattern is characteristic of displacement flows in compliant geometries [9]. By contrast, the large indents on the interface in Fig. 2(a) due to tip-splitting indicate insensitivity to the tapered geometry at low Ca . The distinction lies in the size of the fluid wedge ahead of the interface, which is significantly larger at low Ca . As a result, the effects of the compliance-

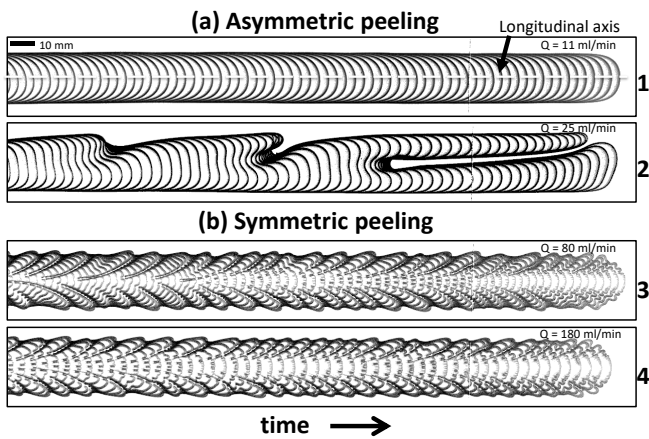


FIG. 2. Composite images of (a) asymmetric and (b) symmetric peeling modes for different values of Q , showing the evolution of the interface. The dashed line indicates the axis of symmetry. The asymmetric mode at $Q = 11$ ml/min propagated steadily with the tip offset from this axis by a small but significant distance of $6 \pm 1\%$ of the channel's width. Images were recorded at fixed time intervals of (from top): 0.50, 0.25, 0.07, 0.05 s. Numbering is consistent between all figures.

induced taper are diminished and the flow is dominated by viscous dissipation within the wedge [see Fig. 1(c)]. The asymmetric fingers at low Ca are associated with the central constriction of the channel ahead of the interface, due to the quartic profile of the collapsed membrane in the transverse cross-section; asymmetric fingers minimise viscous dissipation in rigid channels of similar geometry [25]. Symmetric and asymmetric peeling modes therefore correspond to elastic- and viscous-dominated regimes of reopening, respectively [15].

The pressure of the peeling modes, which is shown with triangles in Fig. 3 as a function of Ca , varies by typically less than the experimental resolution of 10 Pa. This suggests that these modes of propagation are stable in the sense that they persist over the ROI, consistent with peeling modes studied numerically in related geometries [22]. The occurrence of both peeling modes over a similar range of pressures (shaded region) indicates that the system is bi-stable within this band of pressures. The two peeling branches are separated by a range of Ca where we do not observe stable finger propagation. Instead, fingers initiated within that range evolve towards either peeling state through the variation of both their pressure and Ca . The majority of the time-averaged data of these experiments (*filled circles*) shows a clear trend for bubble pressure to decrease with increasing Ca , which is indicative of a pushing branch [Fig. 3]. The large error bars on these transient modes typically reflect a monotonic rise in bubble pressure of 15–40 Pa combined with a fall in Ca , which occur over at least half of the ROI. During this phase, we observe symmetric fingers with high (and increasing) in-plane tip curvature, as shown in the

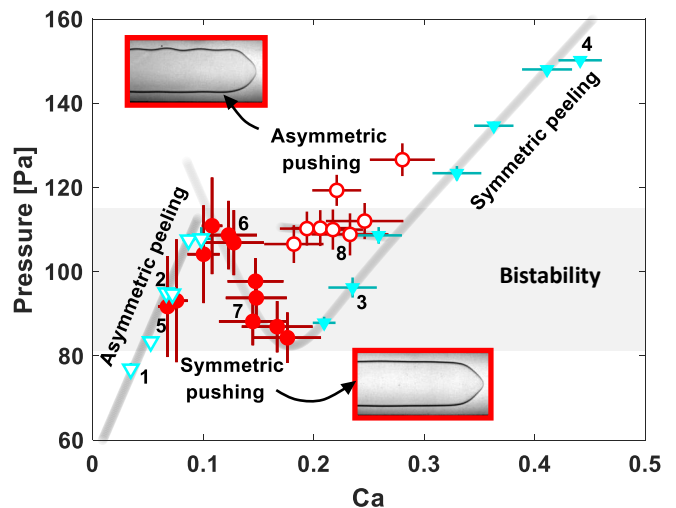


FIG. 3. Bubble pressure as a function of capillary number Ca , showing time-averaged data for peeling modes (*triangles*) and transient modes (*circles*). The band of pressures for which both peeling branches occur is shaded, and the interfacial profiles of pushing modes are inset. Asymmetric modes are indicated by open symbols, and error bars show the standard deviations of experimental measurements.

lower inset image of Fig. 3. The transient observation of these symmetric pushing modes suggests that they are unstable, as in numerical studies which predict continuous accumulation of fluid in the wedge ahead of the interface [22]. The anomalous group of points at higher Ca (*open circles*) are associated with a similar interface, although here the shape has a definite asymmetry, visible in the upper inset image of Fig. 3. We refer to these as asymmetric pushing modes by analogy.

Fig. 4(a) shows composite images from four representative experiments initiated for values of Ca in the unstable region. While the fingers initially adopt the high curvature profile of the pushing modes identified above, their interfaces evolve as they propagate, transitioning from pushing to peeling modes through distinct evolutions of their interfacial profiles (see highlighted interfaces). The peeling mode selected depends on the flow rate Q , which sets the initial conditions of bubble pressure and Ca , thus determining the basin of attraction in which the system initially lies. To illustrate this, Fig. 4(b) shows the pressure- Ca phase space trajectories of the pushing modes in Fig. 4(a). In all cases, the initial transient behaviour of pushing modes is consistent, with the large monotonic rise in pressure accompanied by a deceleration (reduction in Ca) as fluid accumulates ahead of the tip, increasing viscous resistance. This Ca -pressure relation is consistent with pushing behaviour, indicating that the initial evolution of the system is directed parallel to the pushing branch, an observation corroborated by the retention of the pushing interface over this initial transient. We may therefore classify transient dynamics

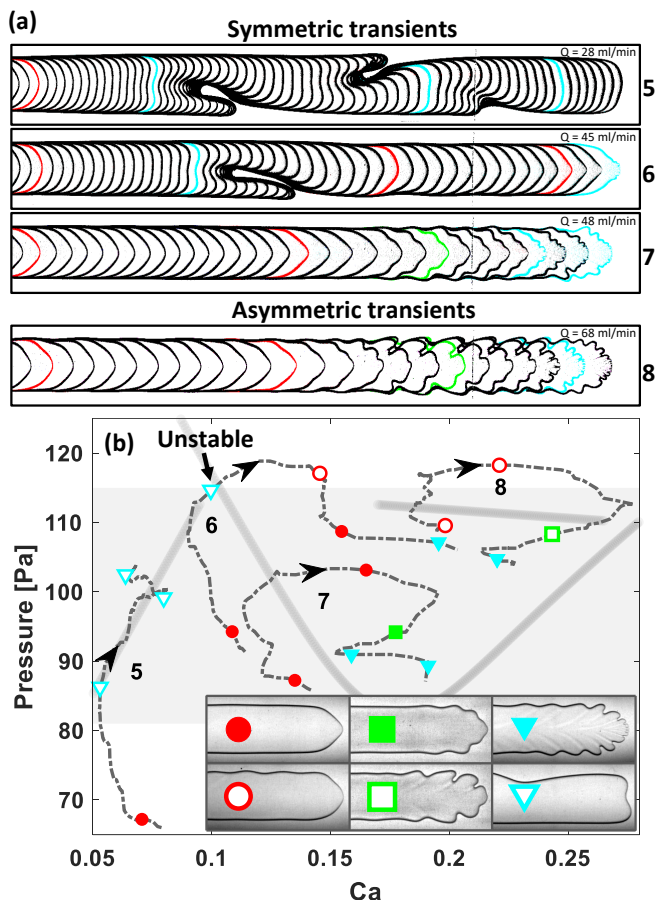


FIG. 4. (a) Composite images showing the transient evolution of fingers towards either the asymmetric or the peeling modes for a range of flow rates Q . Images were recorded at fixed time intervals of (from top): 0.28, 0.20, 0.26, 0.26 s. (b) Time-variation of bubble pressure and Ca for each experiment in (a). Arrows indicate increasing time, and symbols correspond to the highlighted interfaces in (a), with pushing (circles) and peeling (squares and triangles) modes indicated by the key, inset.

both in terms of their interfaces and their pressure- Ca relation at any given time. We will now examine three representative cases, dependent on Q .

At low Q (e.g. experiment 5) the system evolves towards the asymmetric peeling branch, and the interface adopts the flat front associated with this mode. The pressure- Ca relation is then inverted, as the system begins to climb along the peeling branch and we observe tip-splitting. Over the final third of the ROI, both bubble pressure and Ca remain steady to within experimental tolerances, and the asymmetric interface is retained, which suggests that the system has reached a stable state.

At flow rates $Q > 46$ ml/min, however, (e.g. experiments 7 and 8) the system does not converge onto the asymmetric peeling branch. Instead, the system initially follows orbital trajectories, similar to the relaxation oscillations described by [22] for pushing modes in an anal-

ogous 2D system where the in-plane interfacial structure is absent. The mechanisms responsible are likely similar; during the initial transient, the depth of the fluid wedge ahead of the interface increases as fluid is accumulated. This yields a reduction in viscous resistance in this region, and the tip abruptly accelerates as a result. Over this stage, the pushing mode is retained, with the curvature of the tip increasing further, an adaptation which would reduce viscous resistance, allowing fluid in the wedge to escape past the tip. Immediately after, we observe a reduction in both bubble pressure and Ca , consistent with peeling. Over these transients [squares in Fig. 4(b)], we observe the appearance of undulating structures along the previously flat sections of interface either side of the tip. These interface shapes are distinct from either pushing or stable peeling. Their pressure- Ca relation suggests that they may correspond to unstable peeling modes. The dynamics of the system up to this point are therefore dominated exclusively by unstable modes. The final transient is then an abrupt acceleration at fixed pressure, coinciding with a transition to symmetric peeling. These dynamics are robust, qualitatively describing all experiments at $Q > 46$ ml/min.

A distinct dynamical behaviour is observed in experiment 6. At $Q = 45$ ml/min, the system converges onto the asymmetric peeling branch at around the maximum pressure recorded for stable asymmetric peeling modes. The system therefore fails to stabilise and instead returns to pushing modes, first asymmetric then symmetric, before transitioning to symmetric peeling. The repeated interactions with pushing modes, even after visiting a marginally stable peeling mode, suggest that the pushing modes are weakly unstable, thus possessing a high-dimensional stable manifold. Finally, we note that the behaviour of experiment 6 is only observed over a narrow range of Q . At slightly greater or lower Q , the system transitions exclusively to either symmetric or asymmetric peeling. Hence, the results of Fig. 4 suggest that the symmetric pushing mode acts as an organising structure, guiding the system towards either of the stable states and it is therefore an edge state of the system.

In summary, we have observed two stable, but discontinuous peeling branches, mediated over a region of bistability by an unstable pushing branch. This structure is an unambiguous indication of subcriticality, a key component the complex nonlinear dynamics associated with turbulent transition in shear flows [10]. Here, in a flow governed by linear equations, where the nonlinearity is entirely contained within the interface (and the elastic membrane), we have been able to study related dynamics experimentally by direct observation of the interface. This quasi-2D system paves the way for enhanced numerical investigation into subcritical transition. Furthermore, our measurements provide strong evidence of the dominant role of unstable states in the transient evolution of a front-propagating system.

-
- * anne.juel@manchester.ac.uk
- [1] C. Giverso and P. Ciarletta, *Sci. Rep.* **6**, 22610 (2016).
 - [2] A. Brú, S. Albertos, J. L. Subiza, J. L. García-Asenjo, and I. Brú, *Biophys. J.* **85**, 2948 (2003).
 - [3] I. Golding, Y. Kozlovsky, I. Cohen, and E. Ben-Jacob, *Physica A* **260**, 510 (1998).
 - [4] N. M. Schneider, J. H. Park, J. M. Grogan, D. A. Steingart, H. H. Bau, and F. M. Ross, *Nat. Commun.* **8**, 2174 (2017).
 - [5] Y. Couder, in *Perspectives in Fluid Dynamics*, edited by G. K. Batchelor, H. K. Moffatt, and M. G. Worster (Cambridge University Press, Cambridge, 2000) Chap. 2, pp. 53–104.
 - [6] P. G. Saffman and G. Taylor, *Proc. R. Soc. London, A* **245**, 312 (1958).
 - [7] L. Paterson, *J. Fluid Mech.* **113**, 513529 (1981).
 - [8] D. Pihler-Puzović, P. Illien, M. Heil, and A. Juel, *Phys. Rev. Lett.* **108**, 074502 (2012).
 - [9] A. Juel, D. Pihler-Puzović, and M. Heil, *Ann. Rev. Fluid Mech.* **50**, 691 (2018).
 - [10] D. Barkley, *J. Fluid Mech.* **803**, 1 (2016).
 - [11] G. Gallino, T. M. Schneider, and F. Gallaire, *Phys. Rev. Fluids* **3**, 073603 (2018).
 - [12] E. Lajeunesse and Y. Couder, *J. Fluid Mech.* **419**, 125 (2000).
 - [13] D. P. Gaver 3rd, R. W. Samsel, and J. Solway, *J. Appl. Physiol.* **75**, 141 (1990).
 - [14] A. Heap and A. Juel, *Physics of Fluids* **20**, 081702 (2008).
 - [15] L. Ducloué, A. L. Hazel, A. B. Thompson, and A. Juel, *J. Fluid Mech.* **819**, 121 (2017).
 - [16] J. Grotberg and O. E. Jensen, *Ann. Rev. Fluid Mech.* **36**, 121 (2004).
 - [17] M. Heil and A. L. Hazel, *Ann. Rev. Fluid Mech.* **43**, 141 (2011).
 - [18] D. P. Gaver 3rd, D. Halpern, O. E. Jensen, and J. Grotberg, *J. Appl. Physiol.* **319**, 25 (1996).
 - [19] M. Heil, *J. Fluid Mech.* **424**, 21 (2000).
 - [20] A. L. Hazel and M. Heil, *J. Fluid Mech.* **478**, 47 (2003).
 - [21] M. Horsburgh, *Bubble propagation in flexible and permeable channels*, Ph.D. thesis, Cambridge University (2000).
 - [22] D. Halpern, S. Naire, O. Jensen, and D. Gaver, *J. Fluid Mech.* **528**, 53 (2005).
 - [23] L. Ducloué, A. L. Hazel, D. Pihler-Puzović, and A. Juel, *J. Fluid Mech.* **826**, R2 (2017).
 - [24] A. D. McEwan and G. I. Taylor, *J. Fluid Mech.* **26**, 1 (1966).
 - [25] A. Franco-Gómez, A. B. Thompson, A. L. Hazel, and A. Juel, *J. Fluid Mech.* **794**, 343 (2016).